Micromechanics 2000

Volume I

Editor
G. C. Sih

Tsinghua University Press

MESOMECHANICS 2000

Role of Mechanics for Development of Science and Technology

Volume I

Role of Mechanics for Development of Science and Technology

Proceedings of an International Conference of Role of Mechanics for Development of Science and Technology, held at Xi'an Jiaotong University, Xi'an, China, June 13-16, 2000

Edited by

G.C. Sih

Department of Mechanical Engineering and Mechanics,
Lehigh University, Bethlehem, Pennsylvania, USA

Volume I

Tsinghua University Press
Beijing, China

MESOMECHANICS 2000

Proceedings of the Third International Conference for Mesomechanics

Xi'an, P.R. China

Editor: G.C. Sih

Tsinghua University Press

Beijing 100084, P.R. China

Tsinghua

ISBN 7-302-00979-1/0 - 231 Set of 2 Volumes

Numerical simulation of strain rate effects on plastic flow at meso scale level

V.A. Romanova, P.V. Makarov, R.R. Balokhonov

Institute of Strength Physics and Materials Science, Siberian Branch of Russian Academy of Sciences, Tomsk, 634021, Russia

Abstract

Physical mechanics is applied to analyze the dynamic response of strain-rate sensitive material by application of numerical simulation. Two plasticity models that accounts for relaxation properties and surface effects are used. Investigated are the influence of the shock wave amplitude, shock wave front shape and extension rate of the plastic deformation at the meso- and macro-scale level.

1. Introduction

Mathematical models of strain-rate-sensitive metals for the most part were developed for shock wave loading and high-rate extension, torsion, etc. The macroscopic stress relaxation behavior is most pronounced under dynamic loading. Strain rate influence on the elastic precursor decay, stress-strain curves, yield stress and other macroscopic parameters may be determined experimentally and described mathematically. However, stress relaxation at the mesoscale level is important under both high and moderate rates of loading. This is due to inhomogeneity of plastic deformation as a result of the formation of localized shear bands. To be emphasized is that even though macroscopic load is applied at low speed, plastic strain rate in the shear bands may be quite high. The material under study correspond to 1100 and 6061-T6 aluminum alloys.

2. Mathematical definition

2.1 Equations for relaxation medium

To simulate plastic deformation at the mesoscale level, two-dimensional dynamic problem for the relaxation of the elastic-plastic medium was solved by the finite-difference method [1]. Given are the equations of motion

$$\rho \frac{\partial u_i}{\partial t} = \frac{\partial \sigma_{ij}}{\partial x_j} \tag{1}$$

the equation of continuity

$$\frac{\dot{V}}{V} = \dot{\varepsilon}_{ii}, \qquad V = \frac{\rho_0}{\rho} \tag{2}$$

the equations for strain rates

$$\dot{\varepsilon}^T{}_{ij} = \frac{1}{2}\left(\frac{\partial u_i}{\partial x_j} + \frac{\partial u_j}{\partial x_i}\right) \tag{3}$$

and constitutive equations

$$\dot{\sigma}_{ij} = -\dot{P}\delta_{ij} + \dot{S}_{ij} \tag{4}$$

Here, σ_{ij} and ε^T_{ij} are the components of the total stress and strain tensors, respectively. Note that u_i are the components of the particle velocity vector, P the pressure, ρ the mass density and V is the specific volume. The dot indicates time derivative.

Under study is a specimen loaded by weak shock waves and dynamic extension. In this case, heat effect on the pressure is neglected and the medium may be considered as barotropic. That is $P = P(\rho)$. Hence, eqs. (1) to (4) are sufficient without considering the equation of conservation of energy. However, information is needed for heat flow and temperature distribution. The barotropic equation of state for Al is given in [2].

The deviatoric stress components are given by

$$\dot{S}_{ij} = 2\mu\left(\dot{\varepsilon}^T_{ij} - \frac{1}{3}\frac{\dot{V}}{V}\delta_{ij} - \dot{\varepsilon}^p_{ij}\right) \tag{5}$$

where μ is the shear modulus. The plastic strain rates are defined as

$$\dot{\varepsilon}^p_{ij} = \frac{3}{2}\frac{\dot{\varepsilon}^p_{eff}}{\sigma_{eff}} S_{ij} \tag{6}$$

where

$$\dot{\varepsilon}^p_{eff} = \frac{\sqrt{2}}{3}\sqrt{\left(\dot{\varepsilon}^p_{11} - \dot{\varepsilon}^p_{22}\right)^2 + \left(\dot{\varepsilon}^p_{22} - \dot{\varepsilon}^p_{33}\right)^2 + \left(\dot{\varepsilon}^p_{33} - \dot{\varepsilon}^p_{11}\right)^2 + 6\left(\dot{\varepsilon}^p_{12}{}^2 + \dot{\varepsilon}^p_{23}{}^2 + \dot{\varepsilon}^p_{31}{}^2\right)} \tag{7}$$

and

$$\sigma_{eff} = \frac{1}{\sqrt{2}}\sqrt{\left(S_{11} - S_{22}\right)^2 + \left(S_{22} - S_{33}\right)^2 + \left(S_{33} - S_{11}\right)^2 + 6\left(S^2_{12} + S^2_{23} + S^2_{31}\right)} \tag{8}$$

In view of eq. (6), eq. (4) may be rewritten as

$$\dot{S}_{ij} = 2\mu\left(\dot{\varepsilon}^T_{ij} - \frac{1}{3}\frac{\dot{V}}{V}\delta_{ij} - \frac{3}{2}\frac{\dot{\varepsilon}^p_{eff}}{\sigma_{eff}} S_{ij}\right) \tag{9}$$

Eq. (9) implies that relaxation behavior of the deviatoric stress components S_{ij} is the same as that for the effective stress. The viscous relaxation model given in [3] may be used such that the deviatoric stress components become

$$\dot{S}_{ij} = 2\mu\left(\dot{\varepsilon}_{ij}^{T} - \frac{1}{3}\frac{\dot{V}}{V} - \frac{1}{2\eta}\left(1 - \frac{\sigma_o'}{\sigma_{eff}}\right)S_{ij}\right) \tag{10}$$

Here, $\sigma_o' = \sigma_o'\left(\varepsilon_{eff}^{p}\right)$ is the yield stress. The relaxation function $\eta = \eta\left(\sigma_{eff}, \varepsilon_{eff}^{p}\right)$ has been obtained for the 1100 and 6061-T6 aluminum alloys in [3,4].

2.2 Plasticity models

To simulate the elastic-plastic behavior of mesovolume under shock wave loading and extension, use will be made of two plasticity models. The traditional plasticity model (TPM) uses the Mises's yield criterion [1]. Plastic deformation is assumed to occur in any cell of the computational grid when local stress state reaches the yield condition.

The second is a mesomechanical plasticity model (MPM). It accounts for the interface and surface effects on the development of plasticity. According to experimental results of crystal plasticity [5-7], plastic shear originates at the surface and interface of internal structure elements. Plastic shears then propagate through the crystal accompanied by elastic deformation. Based on such a notion, a plastic flow criterion for a computational cell was developed in [4] using continuum and discrete mechanical approaches. The algorithm presented in Fig. 1 describes the state of computational cell at each load step. More specifically, Fig. 1(a) shows the surface of a polycrystalline specimen marked by computational grids. Cells with different shades correspond to different mechanical characteristics. The surface and interface cells are marked with "x" and "dot", respectively. A flow chart of the algorithm shown in Fig. 1(b) describes how the elastic-plastic behavior of a computational cell could be found. Note that σ_{cr} is the critical stress of plastic shear generation, σ^* the theoretical shear strength, ε_{cr}^{p} the critical plastic strain in a neighboring cell.

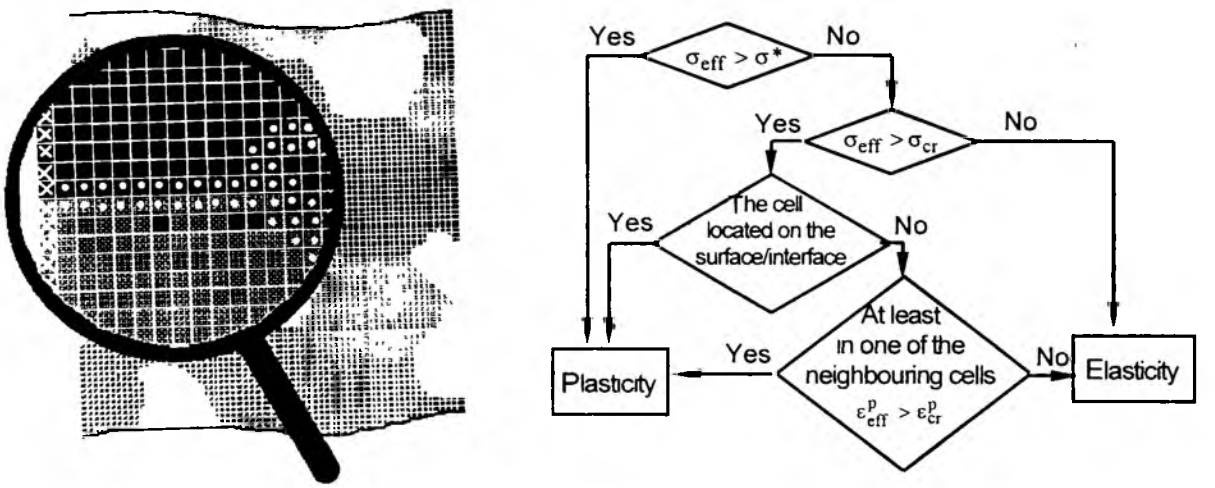

(a) Computational grid (b) Algorithm

Fig. 1 Computer simulation of elastic-plastic development

3. Numerical results and discussion

3.1 Shock wave loading

Strain-rate sensitive 6061-T6 Al alloy under weak shock waves has been investigated. Eqs. (1) to (4) and (10) are numerically solved in terms of Lagrangian variables using the finite-difference method with the second order of accuracy [1]. The polycrystal under calculation consists of grains, which vary in the yield stress and relaxation time. Fig. 2(a) shows a schematic of the plane shock, with the area under calculation being marked. The calculation grid with rectangular cells is marked on the area, Figs. 2(a) and 2(b). Assume that the reflective waves in the specimen can be ignored. A condition of compression thus prevails. Hence, the average strain do not exceed a few percent.

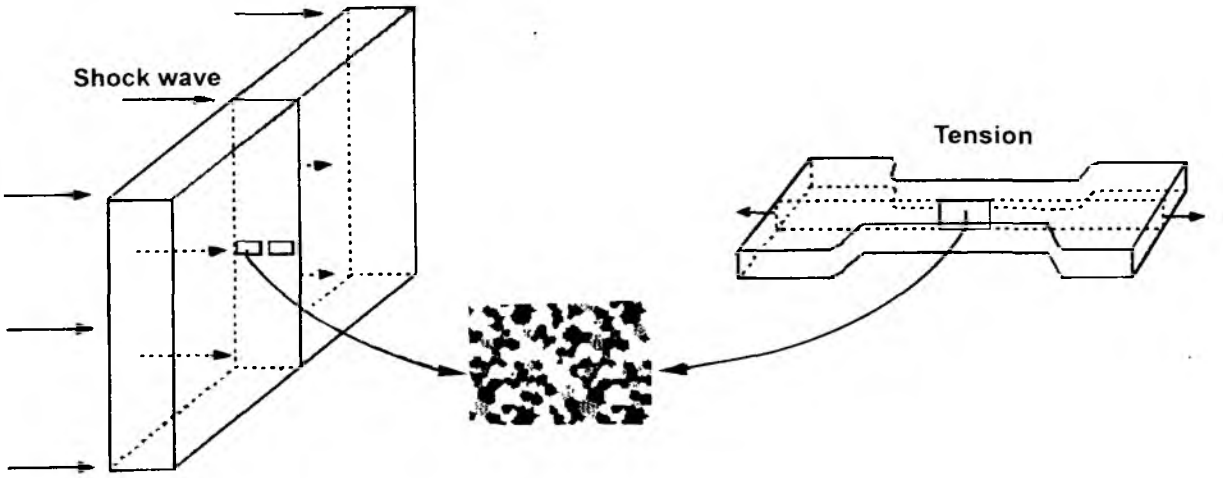

(a) Plane shock (b) Investigated region (c) Tension specimen

Fig. 2 Schematic of dynamically loaded specimen

TPM-calculation. Traditional plasticity model has been used to investigate shock wave amplitude and shape effects on the plastic strain pattern. Revealed are the following features:

- Under compression, the plastic strain localization is attributed to individual grain and grain conglomerate rotations. They are caused by high gradient of shear stress through the shock wave front, Fig. 3(a). Deviation of the particle velocity field from the homogeneous specimen is shown in Fig. 3(b).
- The localized plastic strain pattern depends on the shock wave front shape. Near the impact surface, the shock wave front is extremely narrow and has a steep ascent. Refer to Fig. 4(a) for the stress amplitudes. The shear stress is elevated but its duration is not long enough to cause the considerable grain rotations and plastic strain localization. Fig. 4(b) shows the plastic strain distribution when the wave front is at 0.1mm from the input surface. As the shock wave propagates away from the impact surface its front becomes wider and more gradual. More structure elements are being rotated and strain localization becomes more pronounced, Fig. 4(c).
- The numerical results show that the shock wave amplitude affects the plastic strain pattern. The higher is the amplitude, the smaller is the structure elements to be formed under the shock wave front. Compare Figs. 5(a) and 5(b).

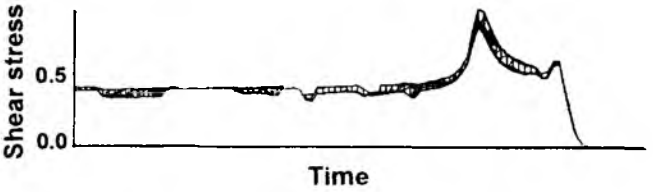

(a) Shear stress

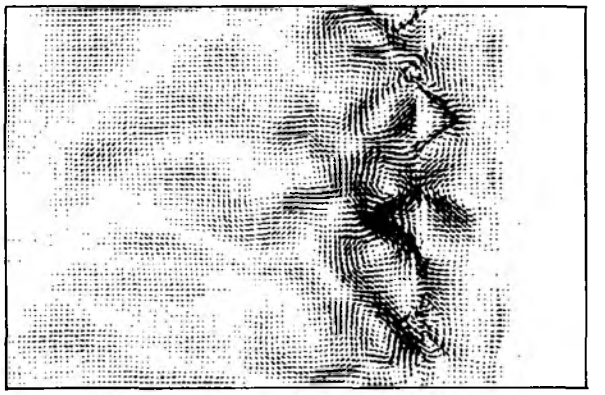

(b) Particle velocity field

Fig. 3 Shear stress and particle velocity field from TPM calculation

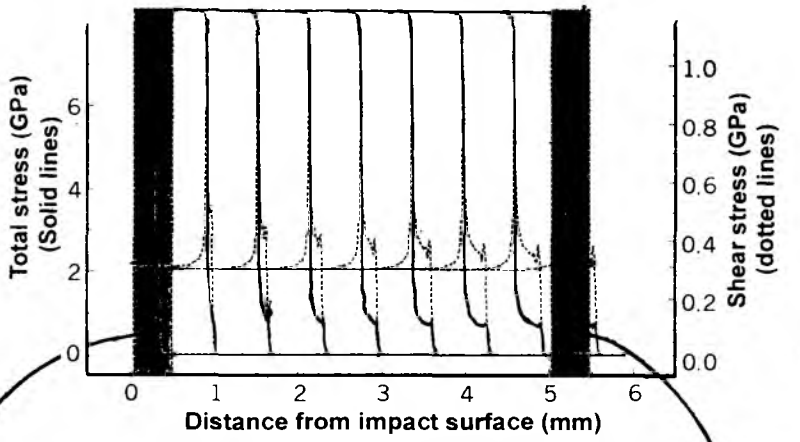

(a) Shock wave profiles

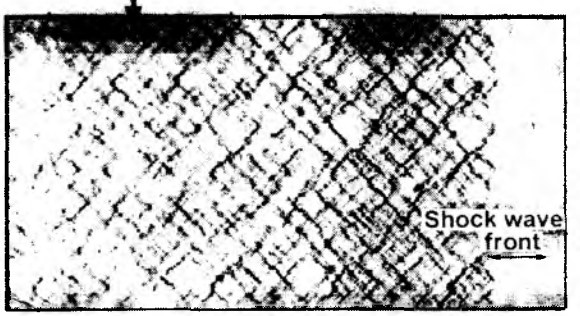

(b) At 0.1 mm

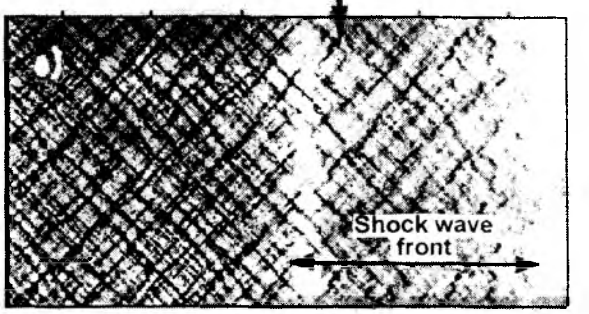

(c) At 5 mm

Fig. 4 Shock wave profiles and plastic strain distribution from impact surface

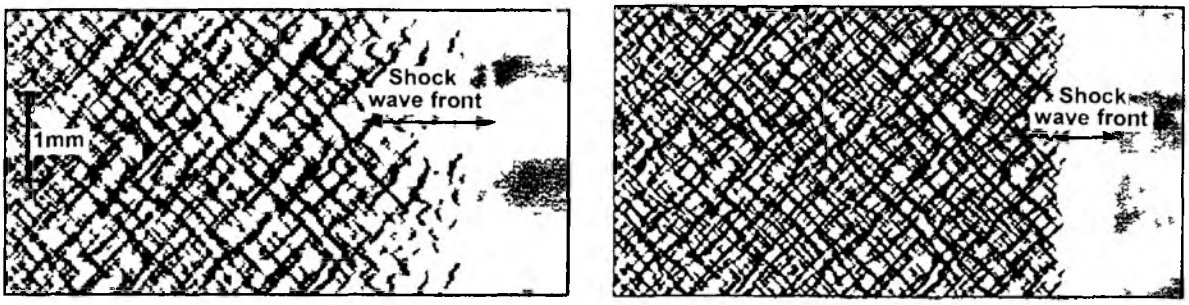

(a) 7 1 GPa (b) 9 GPa

Fig 5 Plastic strain pattern due to shock calculated from TPM calculation

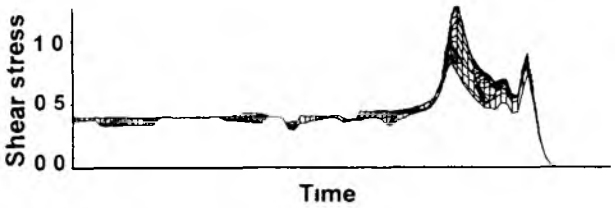

(a)

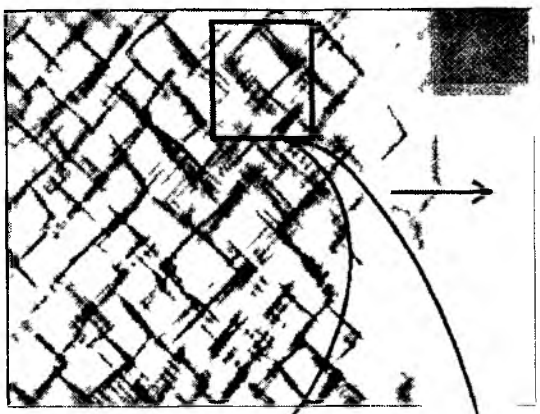

(b) Overall plastic strain

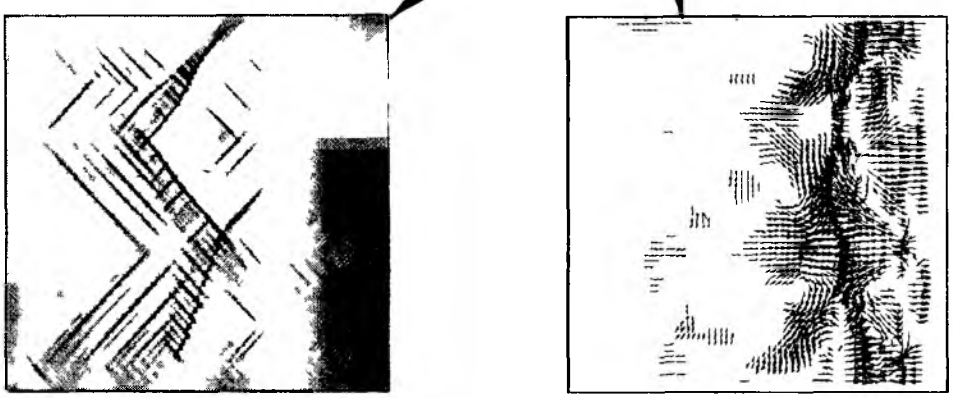

(c) Plastic strain of region A (d) Velocity field of region A

Fig 6 Plastic behavior of polycrystalline specimen under 9GPa shock from MPM calculation

MPM-calculation. The mesomechancis plasticity model is also used to study the intergranular boundary effects and the plastic strain pattern. The specimen is shocked by 9 Gpa. The results show that the plastic shears are generated by the intergranular boundaries. They originate in the elastic precursor and progressively cover the grains in the plastic front. This process constrains the average plastic strain rate and leads to higher average shear stress of the shock wave front than those estimated by TPM. Compare the shear stresses in Figs. 3 and 6. Bands are observed near the grain boundaries after the shock wave front, Fig. 6. Note that Fig. 6(a) shows the rise in shear stress at the wave front. The corresponding plastic strain behavior is displayed in Fig. 6(b). The region A is enlarged in Fig. 6(c) with the velocity field given in Fig. 6(d) for the case of a 9Gpa shock. The same pattern were not found from the TPM calculation.

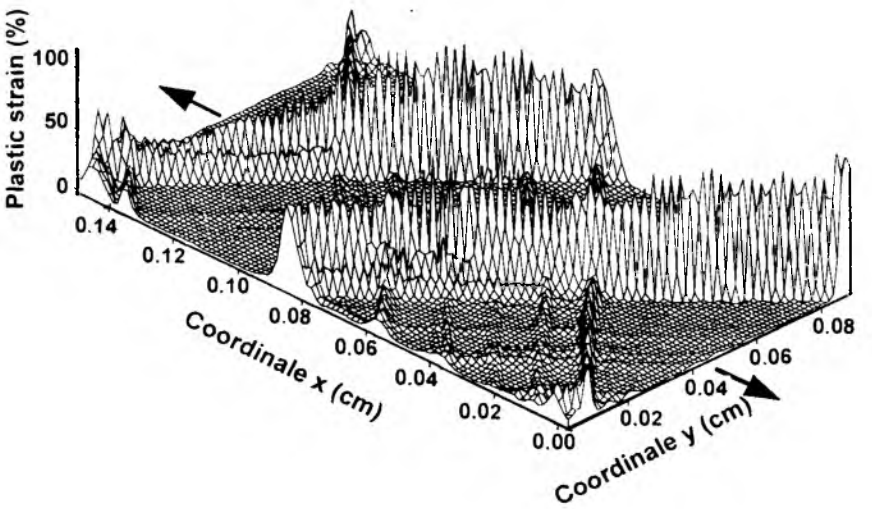

(a) 1.0 (1/s)

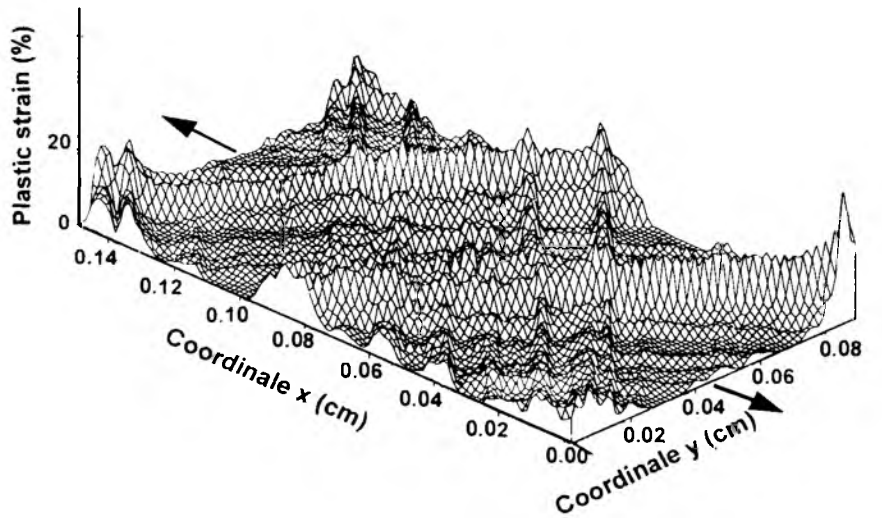

(b) 850 (1/s)

Fig. 7 Plastic strain distribution for different extension rates from TPM calculation

3.2 High tension rate

TPM-calculation. Calculated is a part of polycrystalline specimen under high-rate of tension, Fig. 2(b) and 2(c). A schematic of the tension is shown in Fig. 2(c). The polycrystal under study has the macroscopic mechanical properties of the strain-rate sensitive 1100 aluminum alloy. A numerical procedure was applied to calculate the shock wave loading effects. Results from the TPM-calculation for tensile loading ion at the different rates are presented in Figs. 7 and 8.

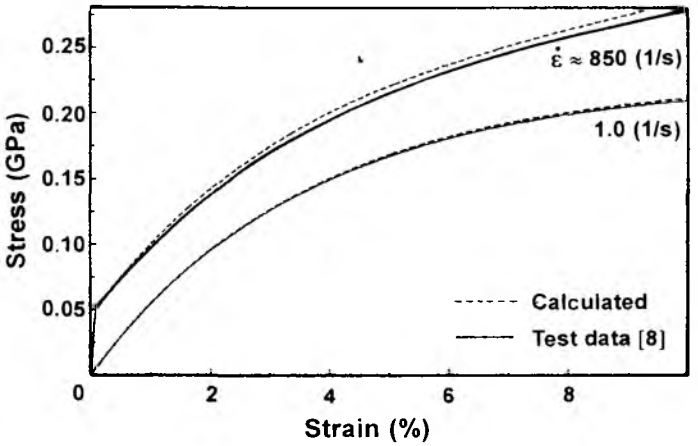

Fig. 8 Comparison of TPM results with test data

Mechanisms of mesoscale plastic strain localization under tension differ from those under shock wave loading. Polycrystal in tension tends to separate in the blocks that undergo shear and rotation. The corresponding plastic strain distributions are displayed in Figs. 7(a) and 7(b) for extension rates of 1 and 850 1/s, respectively. The higher is the extension rate, the greater is the localized band with less severe plastic strain. Compare Figs. 7(a) and 7(b). The phenomenon is attributed to the relaxation properties of material. It should be emphasized, however, that the inclusion of heat may well yield a different pattern of plastic deformation.

The stress-strain curves for 1100 aluminum at different rates are presented in Fig. 8. The higher is the load rate, the higher is the displacement of the appropriate curve in stress. The calculated results are in good agreement with the data in [8].

MPM-calculation. No information for surface/interface influence on plastic strain were obtained from TPM calculation. The MPM were thus used to model the polycrystalline material, Fig. 2(c). The plastic shear generation was modelled on the surfaces and grain boundaries. Stresses of plastic shear generation in the surface cells were found to be lower than those in the grain boundary cells. The interior cells of grain develops plasticity according to the algorithm presented earlier. Calculations are made for plastic deformation developed at an extension rate of 72 s^{-1}. Plastic shear were generated on the surface. The elliptically shaped plastic fronts propagate from the surface perpendicular to the direction of tension, Fig. 9. A smaller substructure is observed inside the plastic zones, Fig. 9(b). Its appearance is attributed to the inner heterogeneity of the polycrystalline structure. Rotation of the mesoscale structure elements are observed near the plastic fronts.

The mesoscale plastic deformation develops in a stepwise fashion. Periods of fast and slow propagation of the bands alternate. The fast propagation of plastic deformation leads to the macroscopic stress relaxation; it corresponds to the declining portion of the macroscopic

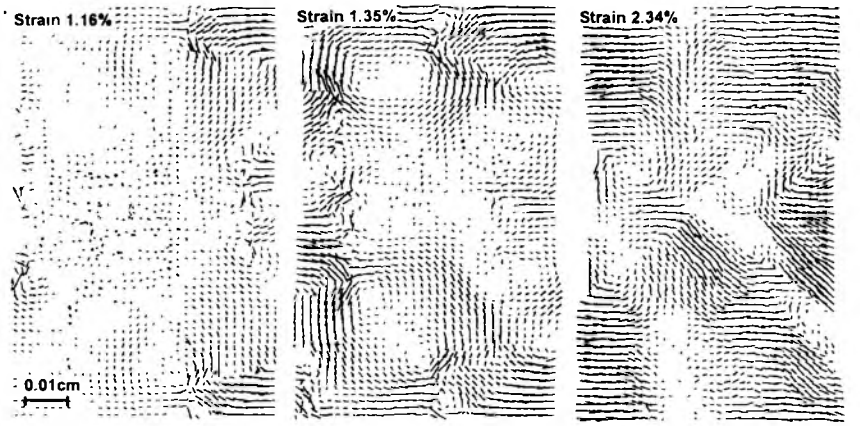

(a) Velocity fields

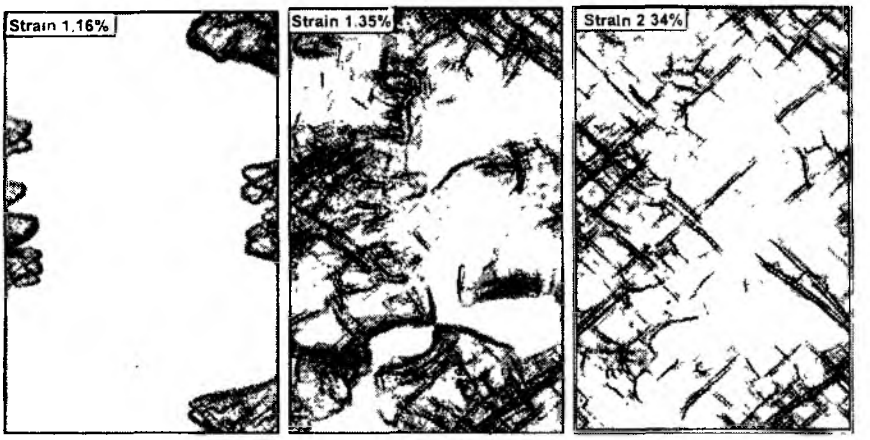

(b) Plastic strain patterns

Fig. 9 Results from MPM calculation for different strains

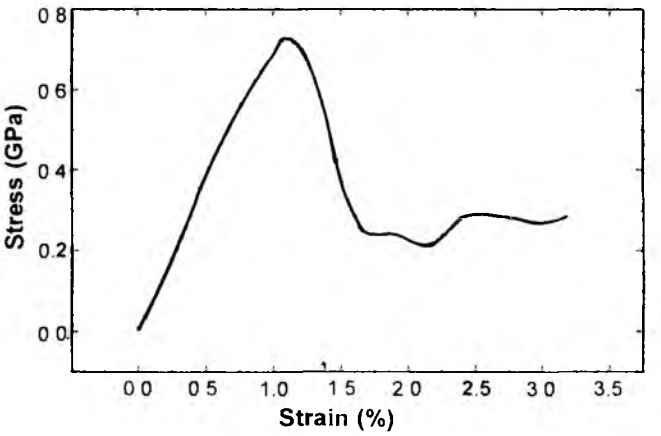

Fig. 10 Stress-strain curve from MPM calculation

stress-strain curve in Fig. 10. The rising stress is followed by relaxation. The bands close to the middle of the specimen propagate with increasing velocity. This causes the stress-strain curve to decline progressively. Finally, the curve levels out. This corresponds to specimen

separation into fragments at the mesoscale. Plastic deformation continues to develop in the bands at approximately 45° to the direction of tension. Mesofragments due to shear prevail. These analytical results agree qualitatively with those observed experimentally in [5,9,10].

4. Conclusion

Presented are the results of numerical simulation of plastic deformation of polycrystalline specimen under shock wave loading and high-rate of extension. Two models of plasticity are used to provide a comparison of results for the relaxation properties of the material and plastic shear generation on the surface. Formation of smaller structure fragments were found to occur for higher shock amplitude and higher extension rate. Also band structures are generated near grain boundaries under shock while surface effects are significant at the mesoscale level under high-rate of extension.

Acknowledgement

Support from the Russian Foundation for Basic Research through the project No. 99–01–00583 is gratefully acknowledged.

References

[1] M. Wilkins, Calculation of elastic-plastic flow, *Methods in Computational Physics*, Vol. 3, (Academic Press, New York, 211-263, 1964).

[2] D.C. Wallace, Equation of state from weak shocks in solids, *Physical Review B.*, 22 (4), 1495-1502 (1980).

[3] T.V. Zhukova, P.V. Makarov, T.M. Platova, etc., The study of viscous and relaxation properties of metals in shock waves by mathematical modeling methods, *J. Physics of Combustion and Explosion*, 23 (1), 29-35 (1987).

[4] V.A. Romanova, *Investigation of Relaxation Processes in Heterogeneous Media by Numerical Simulation Methods*, Ph.D. Thesis, Inst. of Strength Phys. and Mats. Sci., Tomsk, 1999.

[5] E.F. Dudarev, *Microplastic Deformation and Yield Point of Polycrystals*, (Tomsk University Press, Tomsk, 1988).

[6] T. Malis, D.J. Lloyd, K. Tangri, Dislocation generation from grain boundaries in nickel, *Physica Status Solidi (a)*, 11 (1), 275–286 (1972).

[7] L.E. Murr, Some observations of grain boundary leades and leadges as dislocation sources in metals and alloys, *Met. Trans Ser. A.*, 6 (3), 505–513 (1975).

[8] G.V. Stepanov, *Elastic-Plastic Deformation of Materials under the Pulse Loadings*, (Naulova Dumka Press, Kiev, 1979).

[9] V.E. Panin, Foundations of physical mesomechanics, *Physical Mesomechanics*, 1 (1), 5–20 (1998).

[10] Ziegenbein, J. Plessing, H. Neuhaeuser, Mesoscopic studies on Lüders band deformation in concentrated Cu-based alloy single crystals, *Physical Mesomechanics*, 1(2), 5-18 (1998).